Applied Catalysis B: Environmental 339 (2023) 123131

Contents lists available at ScienceDirect

Applied Catalysis B: Environmental

journal homepage: www.elsevier.com/locate/apcatb

Tandem supported Pt and ZSM-5 catalyst with separated catalytic functions for promoting multicomponent VOCs oxidation

Zeya Li, Ruyi Gao, Zhiquan Hou, Xiaohui Yu, Hongxing Dai, Jiguang Deng *, Yuxi Liu *

Key Laboratory of Beijing on Regional Air Pollution Control, Beijing Key Laboratory for Green Catalysis and Separation, Department of Chemical Engineering, Faculty of Environment and Life, Beijing University of Technology, Beijing 100124, China

ARTICLE INFO

Keywords:
Tandem catalyst
Supported catalyst
Multicomponent volatile organic compound
Catalytic oxidation
Polychlorinated byproducts

ABSTRACT

The painting and electronics industries simultaneously release aromatic compounds and chlorinated organics. The development of catalysts with synergistic control of these pollutants is of great significance to achieve air purification. However, developing active catalysts while maintaining good chlorine resistance remain a huge challenge due to the difficulty of the trade-off between the redox properties and acidity and the production of polychlorinated byproducts. Herein, we introduce a novel tandem PtSn/CeO_2&Mn/ZSM-5 catalyst and investigate its catalytic performance for multicomponent volatile organic compounds (VOCs) oxidation. The two individual catalysts, PtSn/CeO_2 and Mn/ZSM-5, were used to catalyze two distinct sequential reactions. PtSn/CeO_2 catalyzed toluene oxidation to produce CO_2 and H_2O. Meanwhile, the introduction of SnO_x favored the adsorption of trichloroethylene (TCE) molecules that prevented Pt sites from chlorine poisoning and possibly converted adsorbed TCE into intermediates, which were subsequently oxidized deeply by the nearby Mn/ZSM-5. This approach resulted in a remarkable oxidation efficiency for toluene (T_{90} = 296 °C) and TCE (T_{90} = 384 °C), with fewer unexpected toxic byproducts (chlorobenzene and 4-chlorotoluene). Furthermore, the tandem catalyst possessed excellent chlorine and water resistances. In conclusion, the above findings provide new insights into the design and/or syntheses of advanced catalysts for widespread VOCs pollution control.

1. Introduction

Urbanization and industrialization have led to a rapid increase in the emissions of volatile organic compounds (VOCs), which has ultimately led to concerns regarding their impact on human health and general well-being [1–3]. In addition, as a kind of detrimental air pollutant with high toxicity, biodegradation difficulty, and a strong capacity for inducing secondary pollution (e.g., photochemical smog), chlorinated volatile organic compounds (CVOCs) cause major concern for scientists [4,5]. VOCs and CVOCs are often released into the atmosphere together with actual industrial emissions [6]. Although the catalytic oxidation technique for VOCs elimination is effective, enhancing the catalytic stability and simultaneously inhibiting the production of organic byproducts are still a great challenge, especially for the oxidation of multicomponent VOCs including CVOCs.

Currently, Pt-based catalysts show the best catalytic activities for aromatic oxidation [7,8]. However, catalysts containing Pt nanoparticles are extremely susceptible to poisoning by trace amounts of Cl species in the combustion of CVOCs, eventually causing catalyst deactivation. Furthermore, the polychlorinated byproducts formed during the oxidation of CVOCs could be more harmful than the original pollutants [9]. These problems have motivated research on improving the Cl tolerance of catalysts and enhancing the catalytic performances. There are three strategies to alleviate chlorinated organic generation and improve the HCl selectivity: 1) acid sites can be added to promote the formation of HCl. Brønsted acid sites can accelerate the dissociation of C—Cl bonds and provide abundant H atoms to form HCl. Lewis acid sites are favorable for the dissociation of C—H bonds. 2) The redox properties can be optimized to achieve low-temperature complete oxidation of Cl-VOCs and their intermediate products to avoid the Cl_2 formation temperature window. 3) The catalyst structures can be adjusted to protect specific components from direct contact with adsorbed Cl species and promote HCl diffusion by enhancing mass transfer. While some achievements have been made, the inevitable catalyst deactivation caused by the adsorption of Cl species must be addressed to enable the use of Pt-based catalysts.

In recent years, transition and rare earth metal oxide catalysts have been widely used, owing to their low costs, better resistance against Cl

* Corresponding authors.
E-mail addresses: jgdeng@bjut.edu.cn (J. Deng), yxliu@bjut.edu.cn (Y. Liu).

https://doi.org/10.1016/j.apcatb.2023.123131
Received 16 April 2023; Received in revised form 7 July 2023; Accepted 26 July 2023
Available online 28 July 2023

poisoning, and abundant oxygen vacancies [10,11]. CeO_2, $FeMnO_x$, CeO_2–CrO_x–Nb_2O_5, Cr_2O_3–CeO_2, and $CeMnO_x$ catalysts are widely used in the oxidation of CVOCs [12–16]. However, by-products are inevitably produced, causing the yield of HCl to decrease. It has been reported that suitable Brønsted acid sites play a dominant role in the adsorption and activation of CVOCs and can also provide hydride to form HCl, thereby enabling the selectivity to molecular chlorine (Cl_2), and the formation of polychlorinated hydrocarbon (PCH) byproducts can be inhibited. H-type zeolites with high acidity usually exhibit better activity and selectivity. Mn/ZSM-5, $MnCeO_x$/HZSM-5, $CeCrO_x$/HZSM-5, and RuCo/HZSM-5 applied for the catalytic combustion of CVOCs have been shown to exhibit good catalytic performances [17–20]. Furthermore, Zhan et al. reported that under the synergistic effects of a large number of weak and medium acid sites and redox properties, the catalytic performances of $Sn_yMn_{1-y}O_x$ catalyst for vinyl chloride oxidation were significantly improved compared with those of pure SnO_x and MnO_x catalysts [21]. In summary, it is imperative to develop new catalysts that possess suitable acidity, strong redox abilities, and good chlorine resistance.

Recently, tandem catalysts have received much attention because of the multiple and distinct interfaces for the catalysis of sequential reactions, which can improve the selectivity for target products [22–24]. Yang et al. designed a unique nanocrystal bilayer structure formed by two distinct interfaces, CeO_2–Pt and Pt–SiO_2, which effectively catalyzed ethylene to achieve propanal selectively [25]. The superior propanal selectivity could be attributed to the synergy between the two sequential reactions and the altered reaction pathway afforded by the tandem reaction [26]. Kang et al. achieved a highly selective catalytic conversion from syngas to ethanol by triple tandem catalysis [27]. In the two-stage Ce/TiO_2–Cu/CeO_2 system for the deep catalytic combustion of dichloromethane (DCM), the rupture of C—Cl and the total oxidation of CO were physically isolated. This separated arrangement showed an excellent oxidation capability for CO and the byproducts, and it avoided the chlorine poisoning of TiO_2 [28]. To date, there have been no reports on the use of tandem catalysts for the catalytic elimination of multicomponent VOCs.

Enlightened by these observations, we report the design and synthesis of a new generation of tandem catalysts, in which acid–solid supported catalysts are packed on the end of Pt-based catalysts for multicomponent VOCs oxidation. The proposed catalyst was applied for the oxidation of 1000-ppm toluene and 200-ppm trichloroethylene (TCE). Based on the experimental findings of the present work, the tandem catalyst had an superior multipollutant conversion efficiency than the individual catalysts, achieving lower toxic byproduct generation. Furthermore, there was no visible change in the catalytic performance of the two-stage catalyst after the introduction of H_2O, indicating its stability. This finding opens a new path for the design of high-efficiency Cl-tolerant catalysts for multicomponent VOCs oxidation.

2. Experimental

2.1. Catalyst preparation

2.1.1. Synthesis of Pt/CeO_2, and $PtSn/CeO_2$

PtSn NPs were synthesized using the solvothermal method. 0.025 mmol of platinum (II) 2,4-pentanedionate ($Pt(acac)_2$), 0.008 mmol tin chloride dihydrate and 100 mg of polyvinylpyrrolidone (PVP, K-30) was dissolved in *N, N*-Dimethylformamide (DMF) (6 mL), the mixture was stirred at room temperature (RT) for 20 min. Then, a 10-mL Teflon-lined autoclave that contains the above solution is heated at 180 °C for 12 h. After cooling to RT, the solution centrifuged and washed with acetone and ethanol for three times. The as-obtained PtSn NPs are dispersed in 5 mL of ethanol for the preparation of the supported catalysts [29]. For comparison purpose, Pt NPs are also synthesized according to the above preparation procedures.

The as-synthesized PtSn and Pt NPs were loaded on the commercial CeO_2 support. The supported catalysts are prepared according to the following procedures. The as-obtained PtSn and Pt NPs were mixed with CeO_2 (theoretical platinum loading = 1 wt%) in 15 mL of ethanol. After being stirred at RT for 12 h, the solids were separated via centrifugation and dried in a vacuum drying chamber. Then, the dried products and 20 mL sodium hydroxide (2 mol/L) were mixed under stirring at 70 °C for 6 h, and this operation is only for PtSn NPs, which is helpful to the exposure of metallic Pt and favor the VOCs oxidation [30]. The mixed solution is centrifuged and the catalyst are washed with deionized water for three times. Finally, the sample was calcined in a muffle furnace for calcination at 550 °C for 2 h. The as-obtained supported catalysts were denoted as $PtSn/CeO_2$ and Pt/CeO_2.

2.1.2. Synthesis of Mn/ZSM-5

Syntheses of HZSM-5 are described as follows: the commercial ZSM-5 with a Si: Al ratio of 38 was carried out by ion-exchanging four times in a large excess of NH_4NO_3 aqueous solution of (1 mol/L, 30 mL/g) at 80 °C for 6 h and calcined again at 550 °C for 6 h. The MnO_x/HZSM-5 catalysts were prepared by the wetness impregnation method with a theoretical metal loading of 12.0 wt%, where the 12.0 wt% represented the loading amount of Mn. Precisely measured $Mn(NO_3)_2{\cdot}4\ H_2O$ and as-obtained HZSM-5 power were mixed in ethanol, following by continuous stirring for 10 h. The mixture was then dried at 80 °C for 10 h and calcinated at 550 °C for 5 h in static air. The products were denoted as Mn/ZSM-5.

For the tandem catalyst system, the first stage was $PtSn/CeO_2$ and the second stage was Mn/ZSM-5. The two stages of the catalysts had the same mass in the reactor. A little amount of silica sand was placed between the two beds for the separation of two catalysts. The tandem system was donated as $PtSn/CeO_2$ & Mn/ZSM-5. It is necessary to note that the distance between the two stages of the catalysts is not greater than 2 mm. Meanwhile, the two stages of catalysts are at the same distance from the temperature monitoring site, which could ensure that the two stages of the catalysts have the same reaction temperature.

For the physical mixture system, the catalyst was prepared by solid state process that the two catalysts $PtSn/CeO_2$ and Mn/ZSM-5 of the equal quality were mixed and well grinded. The physical mixture catalyst was donated as $PtSn/CeO_2$ + Mn/ZSM-5.

2.2. Catalyst characterization

The physicochemical properties of samples were characterized by the inductively coupled plasma−atomic emission spectroscopic (ICP−AES), powder X-ray diffraction (XRD), transmission electron microscopy (TEM), and X-ray photoelectron spectroscopy (XPS) techniques, laser Raman spectroscopy (Raman), high-angle annular dark field−scanning transmission electron microscopy (HAADF−STEM), element mappings, thermal desorption analysis (TD)−online gas chromatography−mass spectrometry (TD/GC−MS), and temperature-programmed surface reaction (TPSR). The detailed characterization procedures can be found in the Supplementary materials.

2.3. Catalytic activity evaluation

Catalytic performance of the samples for toluene, TCE or (toluene + TCE) oxidation is carried out in a continuous flow fixed-bed quartz tubular microreactor. The reaction feed under the actual conditions is composed of (1000 ppm toluene + 20 vol% O_2 + N_2 (balance)) with or without 200 ppm TCE, and the space velocity (SV) is 40,000 mL/(g h). In the case of water vapor introduction, 5.0 vol% H_2O was introduced by passing the feed stream through a water saturator at 34 °C. The analysis of the concentrations of reactants and products was conducted online by gas chromatography. The balance of carbon in the catalytic system was 98.5 ± 1.5 %. The Cl_2 concentration in the above solution was measured using a chemical titration method, and the Cl^- concentration was analyzed using an ion selective electrode. Toluene and TCE conversion (X %) was calculated according to the formula: $X = (c_{inlet} - c_{outlet})/c_{inlet} \times 100$ %, in which the c_{inlet} and c_{outlet} are the inlet and outlet toluene or

TCE concentrations in the feed stream, respectively.

3. Results

3.1. Catalytic performance

The evaluation results for the catalytic oxidation of 1000-ppm toluene and 200-ppm TCE over the as-obtained catalysts under dry air conditions are shown in Fig. 1, and the corresponding 50 % and 90 % toluene and TCE conversion temperatures (T_{50} and T_{90}, respectively) are listed in Table 1. As shown in Fig. 1 A, the catalytic activities of the PtSn/CeO_2 were much better than those of the Pt/CeO_2, which demonstrated the significant promotive effect of SnO_x on the toluene and TCE oxidation [21,31]. It is worth noting that the toluene catalytic activities of the PtSn/CeO_2 (T_{50} = 269 °C and T_{90} = 308 °C) and Mn/ZSM-5 (T_{50} = 292 °C and T_{90} = 336 °C) were comparable. In contrast, the TCE catalytic activity of the PtSn/CeO_2 (T_{50} = 362 °C and T_{90} = 500 °C) was lower than that of the Mn/ZSM-5 (T_{50} = 333 °C and T_{90} = 398 °C). The PtSn/CeO_2&Mn/ZSM-5 exhibited the highest catalytic activities.

To determine the differences between the tandem catalyst and the single catalysts, qualitative identification of the organic byproducts in the off-gases from the mixed VOCs oxidation reaction was conducted. Though the catalytic activity for mixed VOCs oxidation was only slightly different between the single and tandem catalysts, the intermediates detected were distinct. The temperature T_{90} in Fig. 1 C is the temperature for TCE conversion of over 90 % of the catalysts. Fig. 1 C shows a variety of organic by-products, including carbon tetrachloride (CCl_4), perchloroethylene (C_2Cl_4), benzaldehyde (C_7H_6O), and other aromatic organics. In particular, undesired and hypertoxic by-products, namely chlorobenzene (C_6H_5Cl) (CB) and 4-chlorotoluene (C_7H_7Cl), were not found over the PtSn/CeO_2&Mn/ZSM-5, while they were observed with all other single catalysts. Moreover, it has been reported that CB is an important precursor of dioxin formation, which causes great harm to human health and the environment [32,33]. The generation of the highest amounts of polychlorinated byproducts revealed that severe electrophilic chlorination occurred on these catalysts [34].

3.2. Crystal phase structure, morphology, and surface area

A series of characterization experiments were conducted to reveal

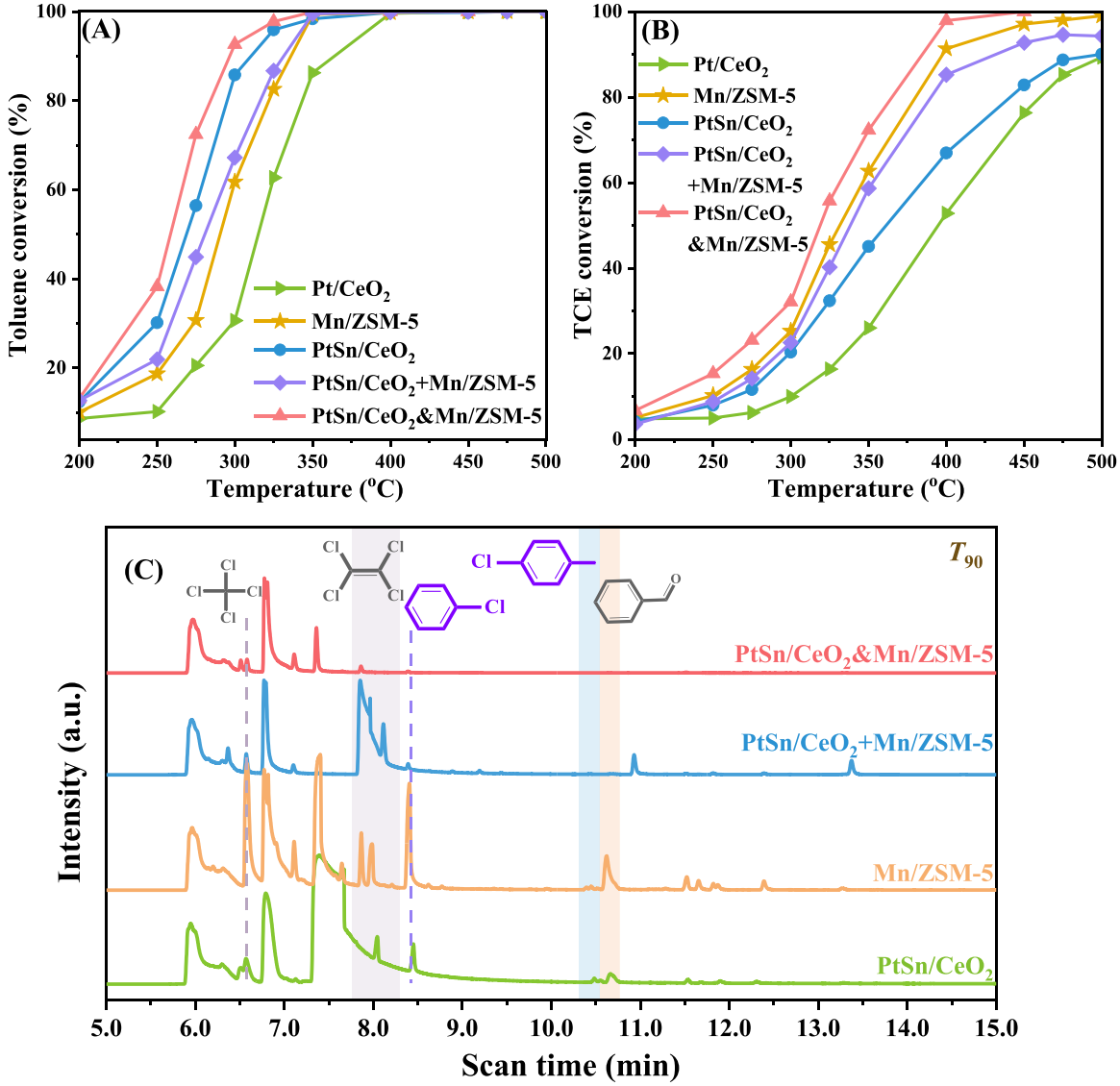

Fig. 1. (A) Toluene and (B) TCE conversion as a function of temperature over the as-obtained samples for the mixed VOCs oxidation. Reaction condition: (1000 ppm toluene + 200 ppm TCE + 20 vol% O_2 + N_2 (balance)), and SV = 40,000 mL/(g h)). (C) qualitative analysis of gaseous by-products generated over the as-obtained samples at the temperature for TCE conversion of 90 %.

Table 1
Toluene and TCE oxidation activities over the as-obtained samples at SV = 40,000 mL/(g h).

Samples	Single toluene oxidation activity (°C)		Activity in mixed VOCs oxidation (°C)							
			Toluene oxidation activity		TCE oxidation activity		Toluene oxidation activity in the presence of H_2O		TCE oxidation activity in the presence of H_2O	
	T_{50}	T_{90}	T_{50}	T_{90}	T_{50}	T_{90}	T_{50}	T_{90}	T_{50}	T_{90}
Pt/CeO_2	—	—	324	375	400	—	—	—	—	—
$PtSn/CeO_2$	219	246	269	308	362	500	276	328	376	500
Mn/ZSM-5	265	297	292	336	333	398	314	344	376	410
$PtSn/CeO_2$ + Mn/ZSM-5	—	—	280	331	335	430	299	339	355	436
Pt/CeO_2&Mn/ZSM-5	—	—	267	398	315	438	—	—	—	—
Mn/ZSM-5&$PtSn/CeO_2$	—	—	262	299	319	390	270	316	371	431
$PtSn/CeO_2$&Mn/ZSM-5	212	243	258	296	319	384	266	298	328	399

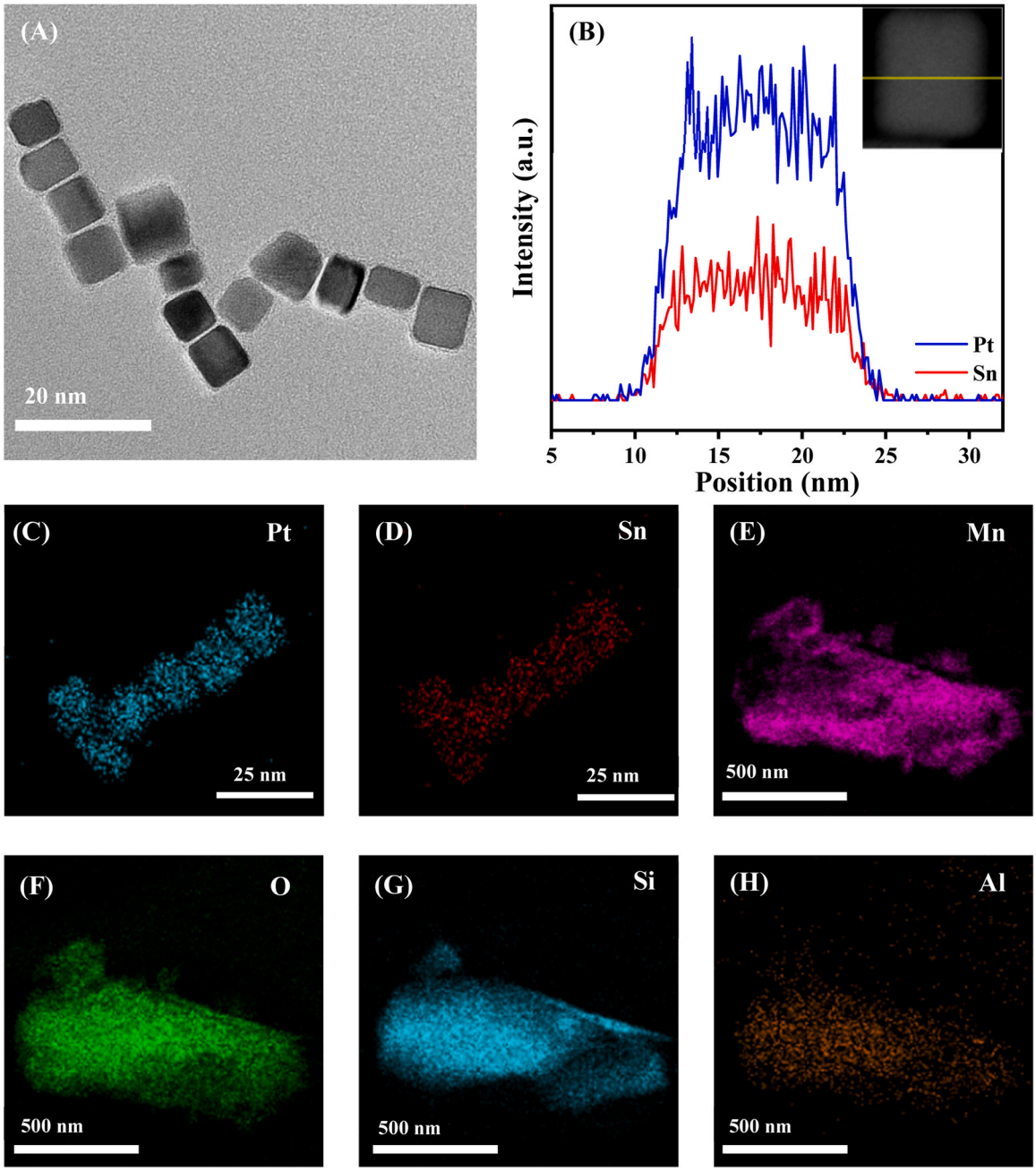

Fig. 2. (A) TEM image of the PtSn NPs, (B) line scan of PtSn NPs, (C, D) EDS elemental mappings of PtSn NPs, and (E–H) EDS elemental mappings of Mn/ZSM-5.

the underlying relationship between the structure and catalytic performances of the as-obtained catalysts. The structures and morphologies of the samples could be measured using transmission electron microscopy (TEM), as shown in Fig. 2. The shapes of the PtSn nanoparticles were regular, while they possessed homogeneous cube-like morphologies. The result of the line-scan analysis and elemental mapping (Fig. 2B—D) indicated that there was a uniform distribution of Pt and Sn species over the entire region. The elemental mappings of the Mn/ZSM-5 (Fig. 2E–H) also revealed that Mn was well dispersed on the surface of the ZSM-5.

Fig. 3 shows the X-ray diffraction (XRD) patterns of the fresh and used PtSn/CeO_2&Mn/ZSM-5 samples after reaction at 400 °C for 30 h. Based on the XRD pattern (JCPDS PDF# 34-0394) of a standard ceria sample, the CeO_2 in all of the samples possessed cubic crystal structures. For the fresh or used PtSn/CeO_2 samples, the XRD pattern was a typical cubic CeO_2 phase, and no characteristic diffraction signals assignable to the PtSn phase were recorded, a result possibly owing to the low loading of the noble metal or high dispersion on the CeO_2 surface. For the Mn/ZSM-5 samples, the peaks corresponding to Mn_2O_3 (JCPDS 41-1442, at $2\theta = 32.9°$ and 55.2°) and ZSM-5 with an MFI-type framework (JCPDS 44-0003, at $2\theta = 7.9°$, 8.8°, 23.0°, 23.9°, 29.8°, and 45.5°) could be clearly observed [35,36].

X-ray photoelectron spectroscopy (XPS) was used to gain insights into the surface elemental compositions of the catalysts, and the corresponding surface elemental molar ratios are listed in Table 2. In the Pt 4 f XPS spectra (Fig. 4A), the asymmetric Pt 4 $f_{7/2}$ and Pt 4 $f_{5/2}$ spectra of each sample could be divided into two components at 70.7 and 72.3 eV and at 73.9 and 76.0 eV, respectively. The signals at 70.7 and 73.9 eV were due to Pt^0 species, while those at 72.3 and 76.0 eV were due to Pt^{2+} species [37–40]. The Pt^0/Pt^{2+} molar ratios (2.96) of the PtSn/CeO_2--fresh were higher than those (0.73) of the Pt/CeO_2-fresh. Previous studies have identified that metallic Pt (Pt^0) species are the active sites for the activation of molecular oxygen at low temperatures, favoring the oxidation of toluene to CO_2 and H_2O [41–45]. Hence, the increase in Pt^0 content may have been one of the reasons for the enhanced PtSn/CeO_2 catalytic activity for toluene oxidation. After the high-temperature reaction, the $Pt^0/Pt^{\delta+}$ molar ratios of the used samples decreased due to the oxidation of platinum species in the oxidizing atmosphere.

Fig. 4B shows the Mn $2p_{3/2}$ XPS spectra of the Mn-containing samples. The Mn $2p_{3/2}$ spectra were asymmetric and could be decomposed into two components at binding energies (BEs) of 643.2 and 641.0 eV,

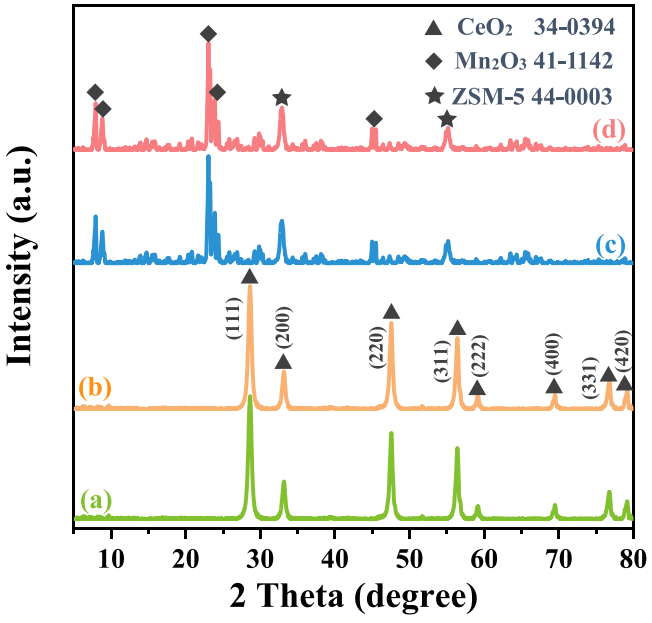

Fig. 3. XRD patterns of the PtSn/CeO_2&Mn/ZSM-5 sample: (a) PtSn/CeO_2-fresh, (b) PtSn/CeO_2-used, (c) Mn/ZSM-5-fresh, and (d) Mn/ZSM-5-used.

which were ascribed to the surface Mn^{4+} and Mn^{3+} species, respectively [46,47]. The Mn^{3+} on the surface, with low valence states of Mn, induced the appearance of surface oxygen vacancies, which favored the adsorption and activation of gas-phase oxygen to highly active oxygen species [48,49]. In addition, in the O 1 s XPS spectra shown in Fig. S2, each sample could be fitted with three oxygen chemical states, with the BEs of surface lattice oxygen (O_{latt}) species at 529.0/529.6 eV, those of surface adsorbed oxygen (O_{ads}, e.g., O_2^-, O_2^{2-}, or O^-) species at 530.6/530.8 eV, and those of surface hydroxyl species at 532.2/532.5 eV [40,50]. In particular, the peak at 532.2 eV of the Mn/ZSM-5 sample was large due to the large number of hydroxyl species on the HZSM-5 surface [51].

For the C 1s XPS spectra shown in Fig. 4C and D, C 1s peak at 284.8 eV was assigned to carbon species adsorbed on the surface as a contaminant. The binding energy at 284.8 eV was related to the C–C bonds of contaminant carbon [52,53]. Furthermore, the presence of surface carbonate species created peaks that appeared at 286.2 and 288.6 eV, which were assigned to C–O and C═O bonds, respectively [44,52,54]. The C–O/C–C ratio was calculated as the ratio of the peak area at 286.2 eV to that at 284.8 eV. It can be seen from Fig. S3(B) and Table 2 that the O_{ads}/O_{latt} and C–O/C–C molar ratios of the used samples increased slightly after the long-term reaction time. This result was due to the accumulation of carbonate species on the surface of the samples during the co-oxidation of CVOCs and VOCs. As shown in Table 2, the Mn/ZSM-5 sample showed the highest C–O/C–C ratio. Similarly, coke deposition on the tandem catalyst and the physical mixture containing the Mn/ZSM-5 sample was observed, while the C–O/C–C ratio of the PtSn/CeO_2 sample was negligible, which indicated that the accumulation of carbonates was more severe on the zeolite catalyst than on the PtSn/CeO_2 catalyst. This result was consistent with the thermogravimetry profile (Fig. S3) of the used catalyst. Fig. S4 shows the three stages of mass loss: 216–276 °C, 379–490 °C, and 612–850 °C. The first stage corresponded to the removal of moisture and physical absorbents (such as toluene and TCE). The weight loss between 379 and 490 °C was mainly attributed to the combustion of coke deposits and the oxidation of chemically adsorbed species on the catalyst surface, while the last stage above 600 °C was associated with the removal of carbonaceous species and the dehydroxylation process of zeolites [55]. During the heating ramp the weight of PtSn/CeO_2 shows very small change with temperature. The higher amount of coke deposition appeared on Mn/ZSM-5 surface.

The Cl 2p XPS spectrum is shown in Fig. S2D, and the surface chlorinity calculated from XPS quantitative results is shown in Table 2. The surface chlorinity reached levels of up to 4.58 %, as shown in Table 2, for the PtSn/CeO_2 sample of the tandem catalyst, which was much higher than the 2.04 % for the Mn/ZSM-5 sample of the tandem catalyst after 30 h of testing. The long-term aging indeed caused Cl species accumulation on the surface of the as-obtained catalysts, while for the Mn/ZSM-5 catalyst, the resulting Cl species reacted with the sufficient H source from the Brønsted acid sites to generate HCl, and thus, the Cl species were easily desorbed from the catalyst.

3.3. Catalytic performance of series of tandem catalysts

To understand the advantages of the tandem catalysts, various tandem catalysts were further investigated. The catalytic activity of the Pt/CeO_2&Mn/ZSM-5 catalyst for the catalytic oxidation of mixed VOCs is shown in Fig. 5 A. It can be seen that in the absence of SnO_x in the catalysts, the toluene oxidation was not affected, but the TCE was not oxidized completely at reaction temperatures below 400 °C. For the Pt/CeO_2&Mn/ZSM-5 catalyst, the TCE conversion reached only 52 % at 400 °C. To better understand the tandem catalysis over PtSn/CeO_2 and Mn/ZSM-5, in a tubular fixed-bed reactor, tandem catalysts of different arrangements were designed, including PtSn/CeO_2 packed in front of Mn/ZSM-5 and PtSn/CeO_2 packed behind Mn/ZSM-5. Similar catalytic behavior was observed for toluene and TCE co-oxidation (Fig. 5B),

Table 2
Actual metal loading of the as-obtained samples and surface element compositions of the fresh and used samples for toluene and TCE co-oxidation at SV = 40,000 mL/(g h).

Samples	Actual metal loadings (wt%)[a]			Surface element composition[b] (mol/mol)					Chlorinity (%)[c]
	Pt	Sn	Mn	$Pt^0/Pt^{\delta+}$	Ce^{3+}/Ce^{4+}	Mn^{3+}/Mn^{4+}	O_{ads}/O_{latt}	C—O/C—C	
Pt/CeO_2-fresh	0.72	—	—	0.73	0.10	—	0.16	0.22	—
$PtSn/CeO_2$-fresh	0.76	0.23	—	2.96	0.10	—	0.20	0.22	—
Mn/ZSM-5-fresh	—	—	8.2	—	—	3.10	0.25	0.22	—
$PtSn/CeO_2$-used	0.76	0.23	–	0.25	0.09	—	0.26	0.28	4.86
Mn/ZSM-5-used	—	—	8.2	—	—	2.89	0.30	1.17	2.12
$PtSn/CeO_2$ +Mn/ZSM-5-used	0.76	0.23	8.2	1.28	0.08	2.86	0.28	1.14	4.33
(PtSn/CeO$_2$)&Mn/ZSM-5-used	0.76	0.23	—	1.69	0.08	—	0.22	0.31	4.58
$PtSn/CeO_2$&*(Mn/ZSM-5)*-used	—	—	8.2	—	—	2.99	0.27	0.96	2.04

[a] Determined by the ICP - AES technique.
[b] Estimated by quantitatively analyzing the peaks in XPS spectra of the samples.
[c] Chlorinity (%) is obtained from XPS quantitative result.

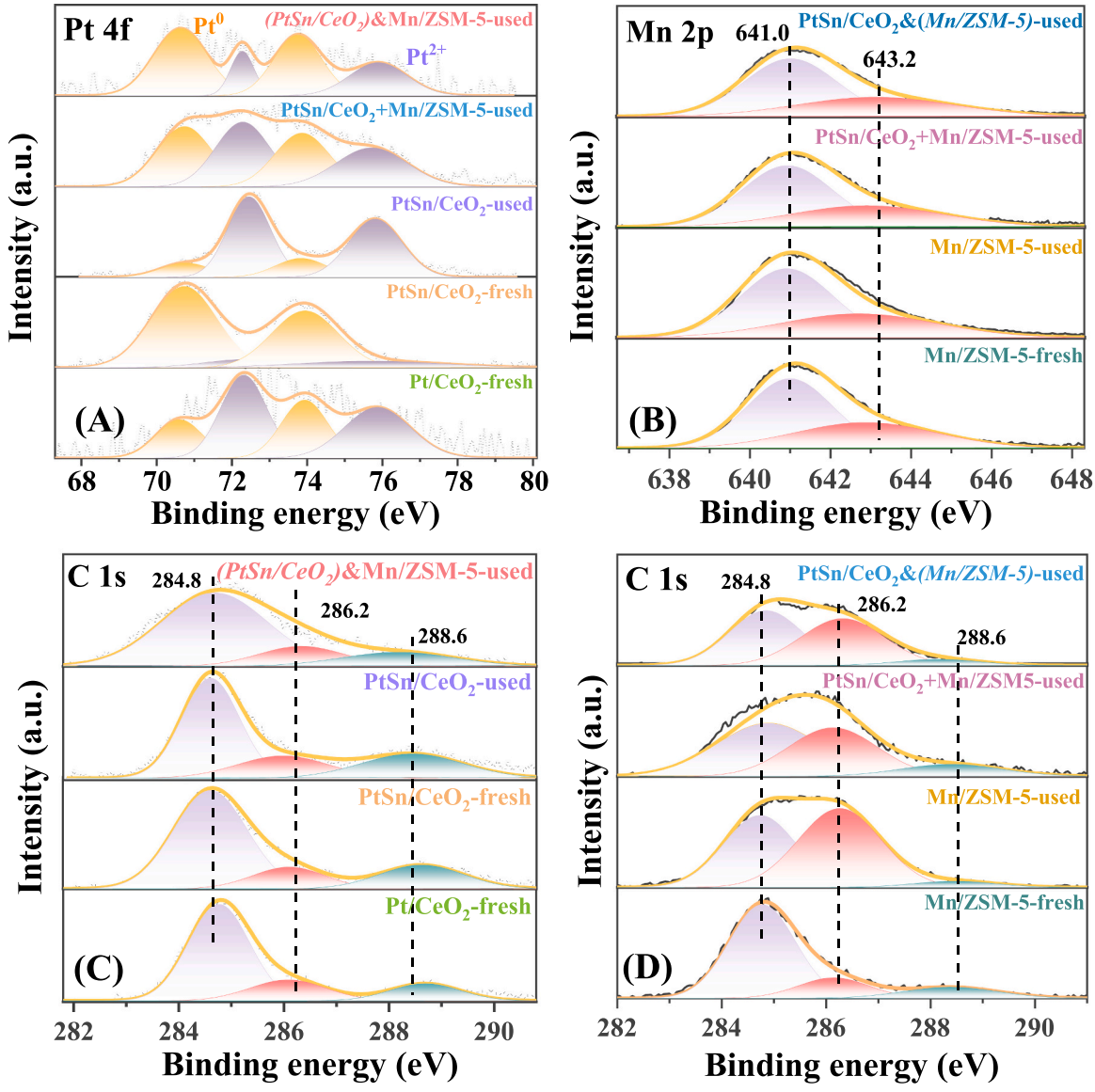

Fig. 4. (A) Pt 4 f, (B) Mn 2p, and (C–D) C 1 s XPS spectra of the as-obtained samples.

although in the reverse order. For Mn/ZSM-5& $PtSn/CeO_2$, the first stage could achieve highly efficient catalytic oxidation of TCE, and the second stage could help the toluene oxidation. As a consequence, similar catalytic behavior observed for toluene and TCE co-oxidation, although in the reverse order of the $PtSn/CeO_2$ and Mn/ZSM-5 catalyst. However, different oxidation priority over $PtSn/CeO_2$&Mn/ZSM-5 and Mn/ZSM-5&$PtSn/CeO_2$ led to distinct product distribution, as shown in Fig. 5 C. The selective temperatures over the different catalysts varied when the

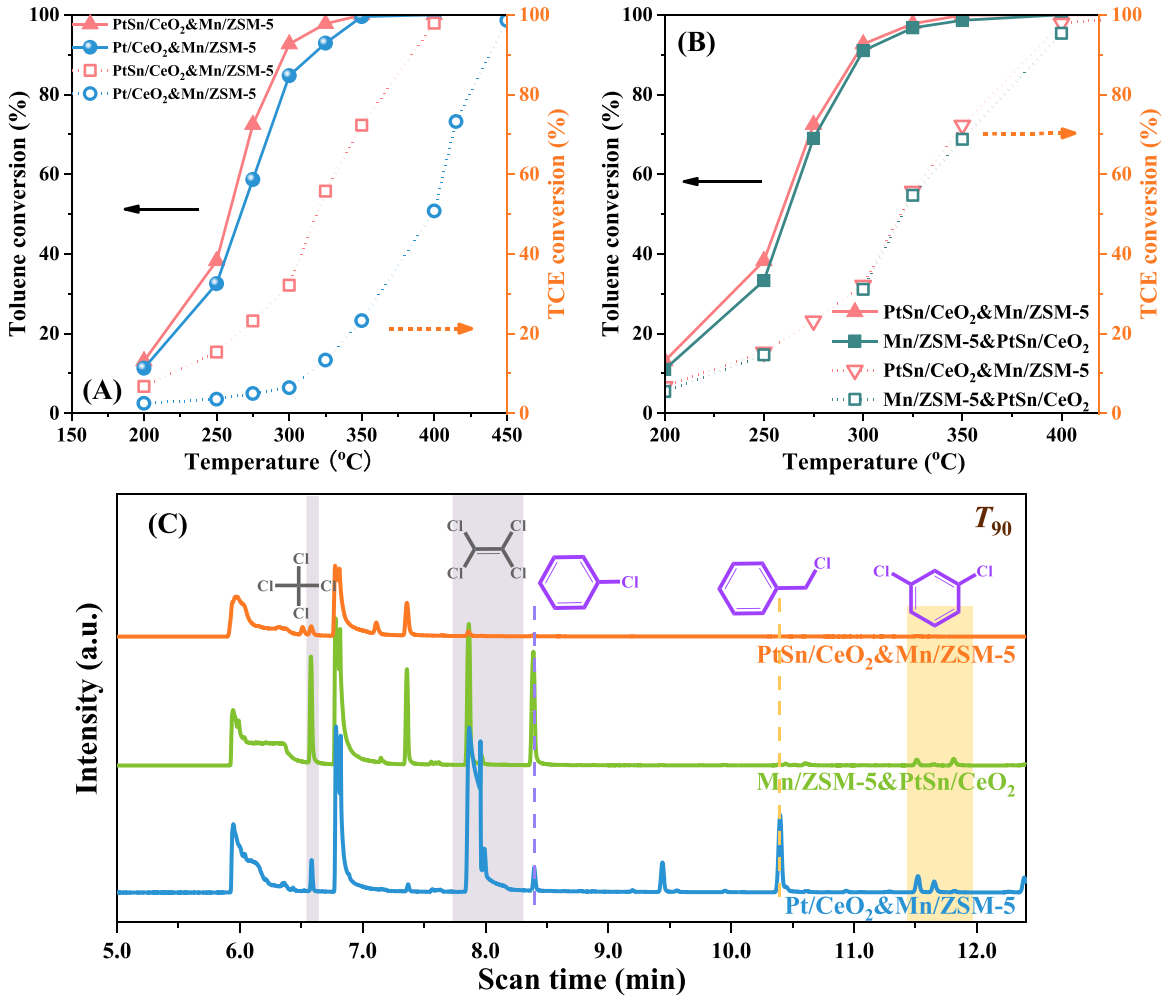

Fig. 5. (A) Toluene and (B) TCE conversion as a function of temperature over the as-obtained samples for the mixed VOCs oxidation and SV = 40000 mL/(g h). Reaction condition: (1000 ppm toluene + 200 ppm TCE + 20 vol% O_2 + N_2 (balance)), and SV = 40,000 mL/(g h)). (C) qualitative analysis of gaseous by-products generated over the as-obtained samples at the temperature for TCE conversion of 90 %.

experiments were carried out at a similar TCE conversion of 90 %. The Mn/ZSM-5&PtSn/CeO_2 samples and the Pt/CeO_2& Mn/ZSM-5 samples both produced a number of unexpected byproducts, including CB, 1,3-dichlorobenzene, and 4-chlorotoluene. The above results indicate that the introduction of SnO_x was beneficial to the TCE oxidation, and tandem catalysis could provide an opportunity to develop an efficient catalytic process to achieve a high catalytic activity and inhibit toxic by-product generation in a single reactor using a tandem catalyst composed of a Pt-based catalyst and an acid–solid catalyst.

The temperature-programmed surface reaction (TPSR) technique was used to investigate the desorption–oxidation behaviors of toluene and TCE over the two individual catalysts, the physical mixture of the catalysts, and the tandem arrangement of the two individual catalysts at 100–900 °C, and the results are shown in Fig. 6(E-H). The signals with $m/z = 91$ and 130 were assigned to desorption of the strongly chemisorbed toluene and TCE species, respectively. Similarly, the desorption temperature of toluene species was higher than that of TCE species on all as-obtained samples, indicating that toluene species were more strongly adsorbed than TCE species on the as-obtained samples. Compared with the PtSn/CeO_2 catalyst, a much higher toluene desorption intensity and higher desorption temperature were observed over the Mn/ZSM-5, PtSn/CeO_2 +Mn/ZSM-5, and PtSn/CeO_2&Mn/ZSM-5 samples, suggesting that the interactions between the reactants and Mn/ZSM-5 were much stronger than those between the reactants and PtSn/CeO_2. This was likely because the HZSM-5 possessed a unique porous structure and abundant acid sites, leading to good toluene and TCE adsorption abilities. CO_2 is one of the target products of VOCs combustion. There were two CO_2 desorption peaks over the PtSn/CeO_2 +Mn/ZSM-5 and PtSn/CeO_2&Mn/ZSM-5 samples centered at 120–122 °C and 250–265 °C, respectively in Fig. 6 G. The former was assigned to the oxidation of toluene with the adsorbed oxygen (O_2^-, O_2^{2-}, or O^-) species, while the latter was assigned to the oxidation of toluene and TCE with the lattice oxygen species. CO_2 was detected in PtSn/CeO_2 and Mn/ZSM-5 at 120 °C and 270 °C, respectively, which indicated that PtSn/CeO_2 played a major role in toluene oxidation at lower temperatures and that Mn/ZSM-5 made a significant contribution to TCE oxidation. Meanwhile, the desorption intensity of HCl was greater on Mn/ZSM-5 than on PtSn/CeO_2, in line with the above conclusions. The CO_2 signals over the PtSn/CeO_2&Mn/ZSM-5 sample increased significantly compared with those over the PtSn/CeO_2 +Mn/ZSM-5 sample, which suggested that the synergistic effect between PtSn/CeO_2 and Mn/ZSM-5 promoted the deep oxidation of toluene and TCE to CO_2 and inhibited the production of byproducts. HCl is the expected final product for TCE oxidation, and its desorption signal ($m/z = 36$) is shown in Fig. 6H. Oxidative dissociation of the C–Cl bonds produced Cl atoms, and the generated Cl atoms combined with the protons on the catalyst to form HCl at low temperatures [56]. HCl was formed on tandem catalysts at lower temperatures, and the peak areas of tandem catalysts were much higher than those of single catalysts, consistent with the evaluation results for the catalytic activities and qualitative identification of organic byproducts, as shown

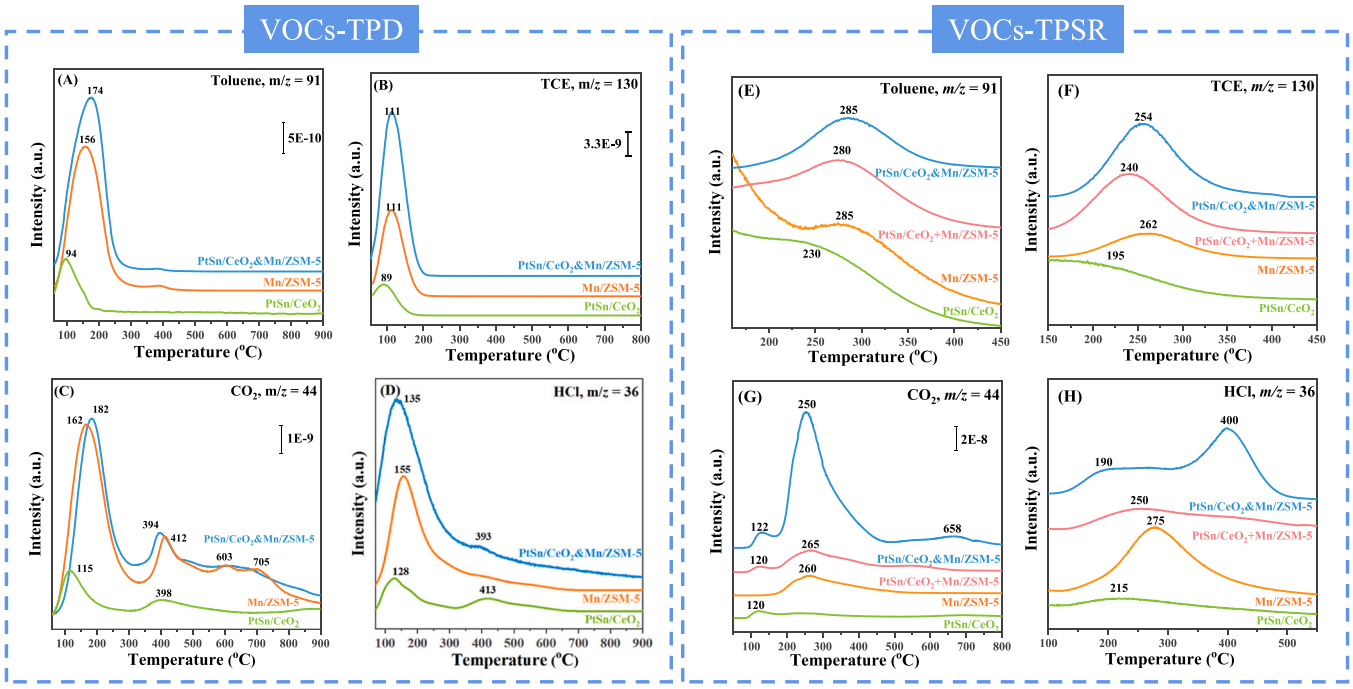

Fig. 6. (A–D) (toluene + TCE)-TPD profiles and (E–H) (toluene + TCE)-TPSR profiles over the different samples.

in Fig. 1. This result confirmed that tandem catalysts with separated catalytic functions can inhibit the formation of byproducts and promote the desorption of Cl-containing species. It can be concluded that the tandem arrangement of the two individual catalysts and the doping of SnO_x increased the catalytic activity and inhibited the production of byproducts.

A comparison of the results for VOCs-TPD and VOCs-TPSR revealed that the toluene and TCE desorption temperatures were increased, while the CO_2 formation temperature was decreased in the presence of O_2, indicating that gaseous oxygen facilitated the oxidation of toluene and TCE. Furthermore, O_2 was introduced during the heating process, and the CO_2 peak area did not show an obvious decrease at low temperatures (below 200 °C). However, the CO_2 peak area increased significantly above 200 °C in the presence of O_2, which was attributed to the gaseous

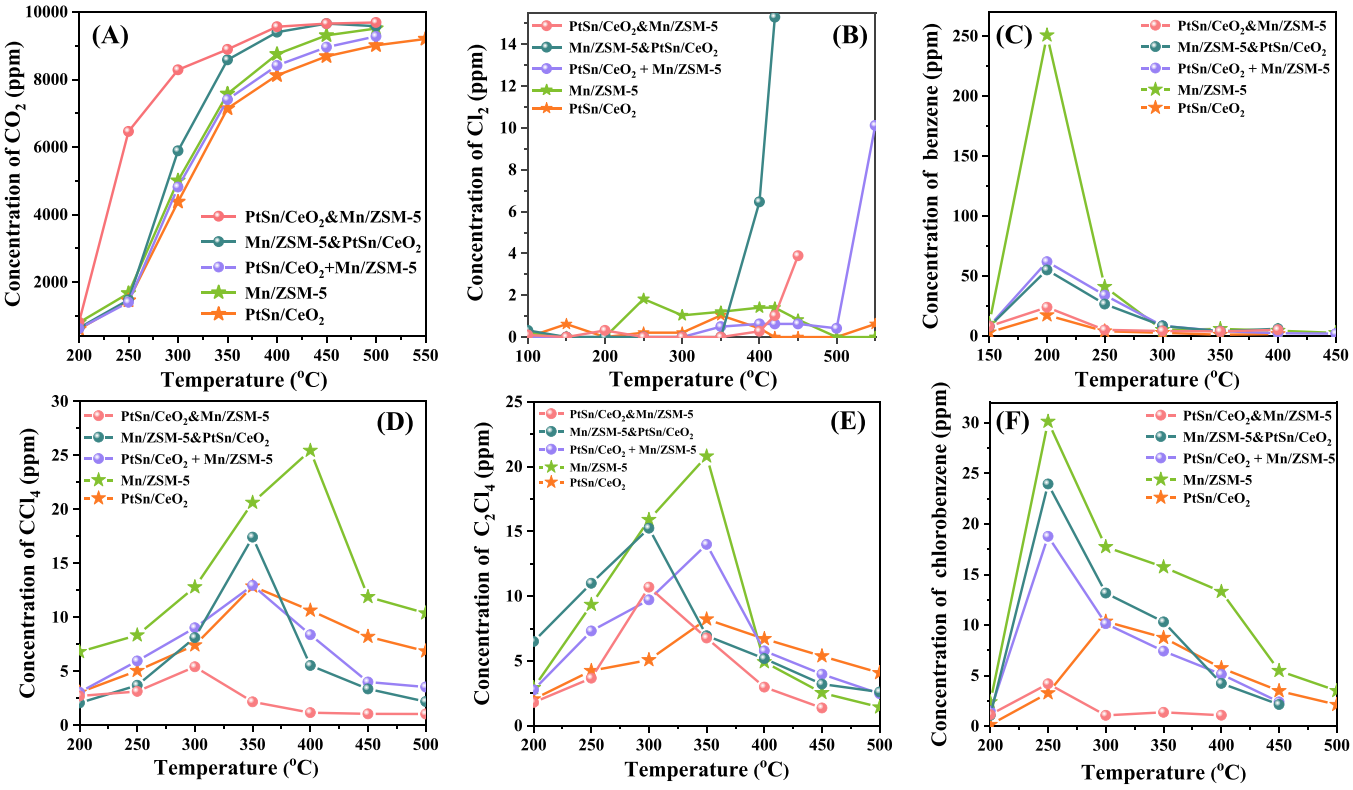

Fig. 7. Product concentration as a function of temperature over the as-obtained samples.

oxygen that played a critical role in the rapid replenishment of active surface lattice oxygen, thus accelerating the oxidation of toluene and TCE.

3.4. Catalyst selectivity and stability

It is necessary to analyze the product selectivity over the different catalysts. The concentrations of a few intermediates, such as benzaldehyde (C_7H_6O) and 4-chlorotoluene (C_7H_7Cl), were too low to detect. Hence, Fig. 7. illustrates the quantitative analyses of the main organic byproducts. The concentrations of byproducts increased with temperature, but when the reaction temperature increased to 350–400 °C, the concentrations of CCl_4 and C_2Cl_4 decreased gradually (Fig. 7D and E), and the concentration of Cl_2 increased rapidly over PtSn/CeO_2 +Mn/ZSM-5 and Mn/ZSM-5&PtSn/CeO_2, which indicated that the decomposition of organic byproducts at high temperature and the occurrence of the Deacon reaction. Furthermore, the concentration of benzene increased at 150–200 °C, and decreased at 200–250 °C (Fig. 7C). In contrast, the chlorobenzene concentration increased at 200–250 °C and decreased at 250–300 °C (Fig. 7F), indicating that benzene is the precursor for the generation of chlorobenzene. The concentrations of byproducts were higher over Mn/ZSM-5 than over other catalysts; this was due to the inadequate oxidation ability of Mn/ZSM-5. For the PtSn/CeO_2 sample, the formation of benzene and chlorobenzene was inhibited. In other words, the PtSn/CeO_2 sample showed better catalytic activities in toluene oxidation at lower temperatures (consistent with the results for VOCs-TPSR), which is favorable for suppressing the formation of chlorobenzene, 1,3-dichlorobenzene, and 4-chlorotoluene.

CO_2 is one of the target products of VOCs combustion. As shown in Fig. 7A, the PtSn/CeO_2&Mn/ZSM-5 exhibited higher CO_2 yields than the other three catalysts, which were comparable to the toluene and TCE conversion trends, indicating that very little toluene and TCE were oxidized to organic byproducts over the PtSn/CeO_2&Mn/ZSM-5 catalyst. In other words, the PtSn/CeO_2, Mn/ZSM-5, and Mn/ZSM-5&PtSn/CeO_2 contributed to CO_2 yields that were apparently lower than the mixed VOCs conversion, revealing that they produced many more organic byproducts than the PtSn/CeO_2&Mn/ZSM-5. HCl and Cl_2 were the final products containing Cl, which could effectively reduce the Cl species deposition on the catalyst surface. Thus, the concentration of Cl_2 was analyzed during the catalytic oxidation of the mixed VOCs. It can be seen that the Deacon reaction became significant at 350 °C (Fig. 7B), where the concentration of Cl_2 increased with temperature and finally reached up to 15.3, 10.1, and 3.9 ppm over Mn/ZSM-5&PtSn/CeO_2, PtSn/CeO_2 +Mn/ZSM-5, and PtSn/CeO_2&Mn/ZSM-5, respectively, at temperatures of 400 °C, 550 °C and 450 °C, respectively. For the PtSn/CeO_2 samples, there was no apparent generation of Cl_2, which may have been because its redox ability was weaker than that of the tandem catalysts and the Cl species could also react with aromatic skeletons, generating CB through the electrophilic substitution [57]. Therefore, polychlorinated byproducts were restrained over PtSn/CeO_2&Mn/ZSM-5 because of reduced Cl_2 formation. Similarly, very little Cl_2 was detected over the Mn/ZSM-5, which may have been due to the Brønsted acidity playing a dominant role in the adsorption and activation of CVOCs, significantly inhibiting the formation of molecular chlorine [58,59].

The selectivity of chlorine-containing products was calculated using the Cl mass balance approach, and the results are shown in Fig. 8. There was a sharp increase in the selectivity of HCl as the temperature increased, which was accompanied by a significant reduction in the formation of byproducts. The PtSn/CeO_2&Mn/ZSM-5 catalyst showed high HCl selectivity, which reached 82.1 % at 328 °C with 50 % TCE conversion and even reached up to 95.6 % at 400 °C with 90 % TCE conversion. However, the HCl selectivity was only 43.9 % over Mn/ZSM-5 at a TCE conversion rate of 50 %. In this study, a large amount of polychlorinated byproducts was detected over MnO_x, which is consistent with a previous study [60].

The stability of catalysts is crucial for industrial applications. Fig. S4D shows the catalytic stability of the PtSn/CeO_2&Mn/ZSM-5 for the mixed VOCs oxidation at 400 °C (toluene and TCE conversion = 100 % at SV = 40,000 mL/(g h)). The toluene and TCE could maintain 100 % conversion for 30 h, indicating that the PtSn/CeO_2&Mn/ZSM-5 sample possessed high resistance to the Cl species. We also examined the crystal structures of the used PtSn/CeO_2&Mn/ZSM-5 sample, and its XRD patterns are shown in Fig. 3. There were no apparent changes in the crystal structures of the PtSn/CeO_2 or Mn/ZSM-5 before and after the long-term experiments.

The formation of water is inevitable during the catalytic oxidation process. Water resistance of a catalyst is also an important factor for

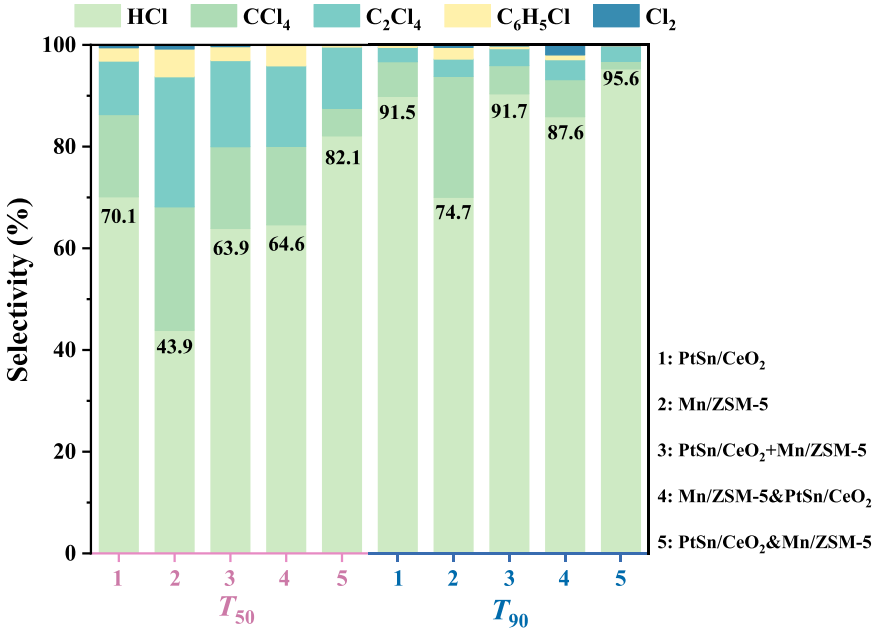

Fig. 8. Selectivity of chlorine containing product over the as-obtained samples at the temperature for TCE conversion of 50 % and 90 %. Reaction condition: (1000 ppm toluene + 200 ppm TCE + 20 vol% O_2 + N_2 (balance)), and SV = 40,000 mL/(g h)).

evaluating the catalyst stability. The effect of 5.0 vol% water vapor introduction on the catalytic performances of the PtSn/CeO_2&Mn/ZSM-5 and PtSn/CeO_2 +Mn/ZSM-5 was investigated, and the results are shown in Fig. S5. It can be seen that there was no significant loss in toluene conversion in the presence of 5.0 vol% water vapor. Simultaneously, the TCE conversion over the PtSn/CeO_2&Mn/ZSM-5 dropped slightly, but the catalytic activity was recovered after water vapor was cut off. In contrast, the TCE conversion over the PtSn/CeO_2 +Mn/ZSM-5 decreased by about 10 % when 5.0 vol% of water vapor was introduced at 335 °C, and the initial value could not be recovered. Similarly, at higher temperatures, the water-resistance abilities of PtSn/CeO_2&Mn/ZSM-5 and PtSn/CeO_2 +Mn/ZSM-5 for the mixed VOCs oxidation were investigated, as shown in Fig. S4(A,B). It became apparent that water had little effect on the mixed VOC oxidation reaction at higher temperatures, which was ascribed to the deep oxidation of VOCs and byproducts at elevated temperatures. Meanwhile, the influence of water vapor on the catalytic activity of the as-obtained samples was investigated. As observed in Fig. 9 A and B, for toluene conversion, the T_{50} of PtSn/CeO_2, Mn/ZSM-5&PtSn/CeO_2, and PtSn/CeO_2&Mn/ZSM-5 decreased by 6–8 °C when 5 vol% of H_2O was added. In contrast, the influence of H_2O on Mn/ZSM-5 and PtSn/CeO_2 +Mn/ZSM-5 was more noticeable (T_{50} decreased by 18–23 °C). Furthermore, the inhibitive effect of H_2O on the catalytic oxidation of TCE became apparent, and the conversion of TCE largely decreased over the Mn/ZSM-5 (T_{50} from 333 °C to 376 °C), PtSn/CeO_2 +Mn/ZSM-5 (T_{50} from 335 °C to 356 °C), and Mn/ZSM-5&PtSn/CeO_2 (T_{50} from 319 °C to 371 °C) catalysts. However, the existence of water vapor could slightly affect the conversion of TCE on the PtSn/CeO_2 and PtSn/CeO_2&Mn/ZSM-5 catalysts. Thus, the PtSn/CeO_2&Mn/ZSM-5 catalyst possessed excellent water resistance ability, indicating that the tandem catalyst has potential for practical industrial applications.

To explain why the tandem catalyst possessed better water-resistance abilities, the effects of water vapor on the formation of organic byproducts were also investigated, as shown in Fig. 10. For the Mn/ZSM-5, PtSn/CeO_2 +Mn/ZSM-5, and Mn/ZSM-5&PtSn/CeO_2 samples, the amounts of generated C_2Cl_4, C_7H_7Cl, and $C_6H_4Cl_2$ increased after the addition of water. In contrast, for the PtSn/CeO_2 and PtSn/CeO_2&Mn/ZSM-5 samples, there was no significant increase in all types of products with the addition of water at the same temperature. According to the above results, the addition of water deactivated the Mn/ZSM-5, PtSn/CeO_2 +Mn/ZSM-5, and Mn/ZSM-5&PtSn/CeO_2 samples, and there was a massive accumulation of intermediates over Mn/ZSM-5, which could be the reason for the deactivation. In other words, the reduced formation of byproducts over PtSn/CeO_2 and the separated catalytic functions of the tandem catalyst are the reasons for the excellent water resistance of the PtSn/CeO_2&Mn/ZSM-5 catalyst.

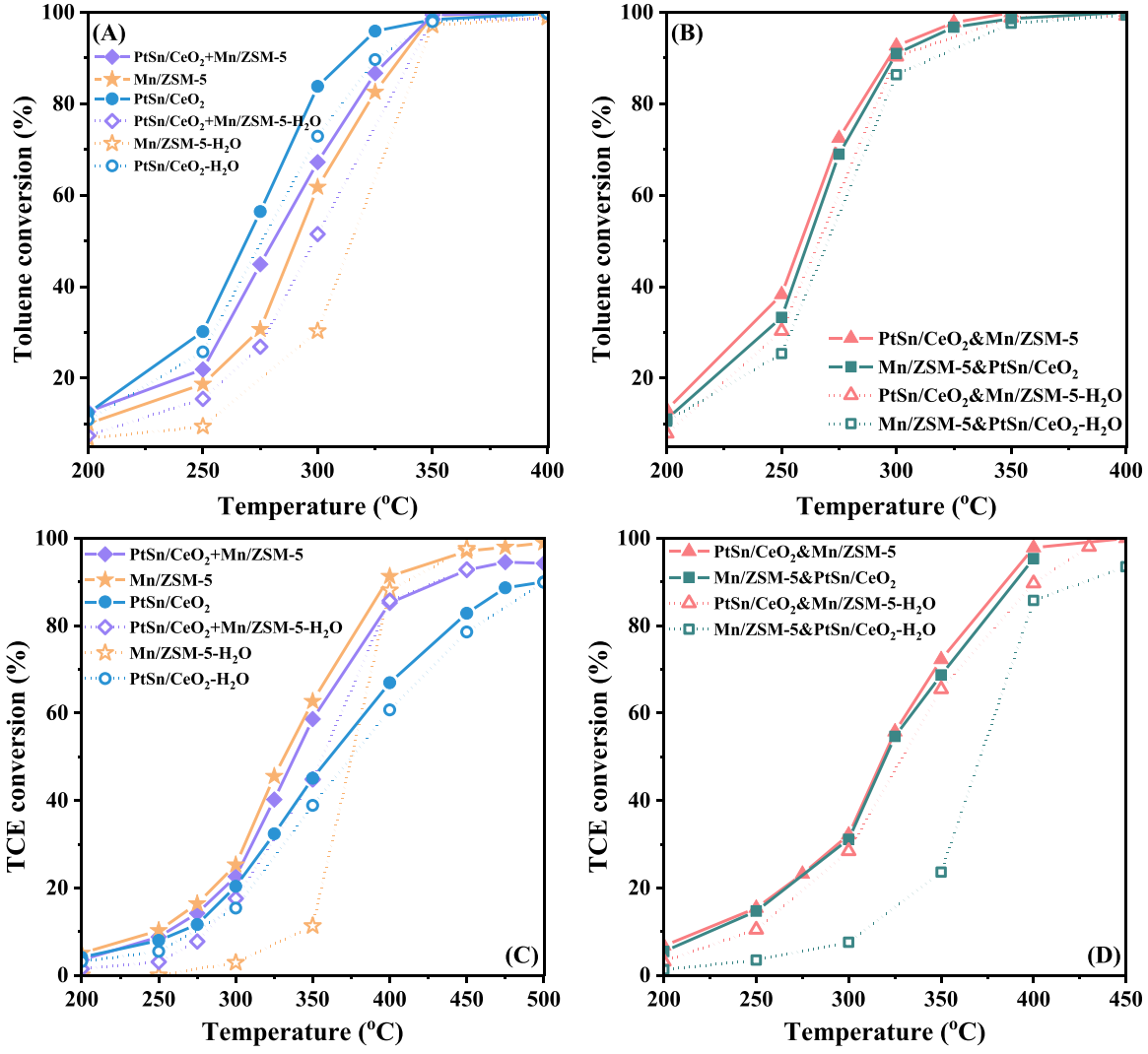

Fig. 9. (A-D) Catalytic activities of the as-obtained samples for toluene and TCE co-oxidation in the presence or absence of water vapor at SV = 40,000 mL/(g h). Reaction condition: (1000 ppm toluene + 200 ppm TCE + 20 vol% O_2 + N_2 (balance)).

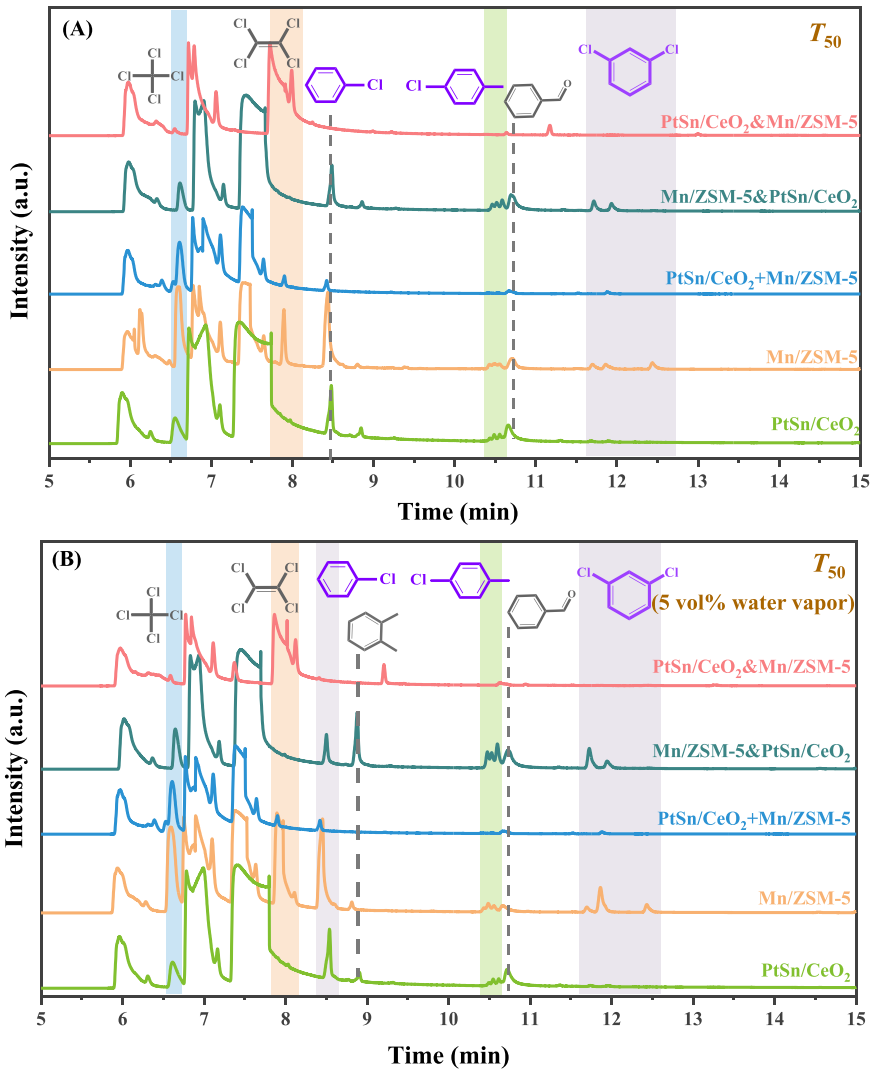

Fig. 10. Qualitative analysis of gaseous by-products generated in the (A) absence and (B) presence of 5 vol% water vapor over the different samples at the temperature for 50 % TCE conversion.

3.5. *Possible reaction mechanism*

Based on the above discussion, a two-step oxidation mechanism for the catalytic combustion of toluene and TCE over the PtSn/CeO_2&Mn/ZSM-5 catalyst was proposed (shown in Scheme 1). There are two possible explanations for why CB, 1,3-dichlorobenzene, and 4-chlorotoluene byproducts were not found for the PtSn/CeO_2&Mn/ZSM-5 catalyst but found for the single catalysts or other tandem catalysts. We can assume that one of the following explains the lack of byproduct formation: a) these byproducts never appeared in the toluene and TCE oxidation, and b) the intermediates were completely oxidized over the second part of the tandem catalyst. These toxic products were still detected on the Mn/ZSM-5&Mn/ZSM-5 samples at 350 °C and 420 °C (Fig. S6), ruling out the second hypothesis. Thus, the two parts of the PtSn/CeO_2&Mn/ZSM-5 catalysts played a vital role in reducing toxic byproducts and in enhancing the catalytic activity for CVOCs oxidation and catalytic selectivity to HCl.

Recent studies have identified that Pt species are the active sites for the activation of molecular O_2, favoring the complete oxidation of toluene to CO_2 and H_2O [41,44,61]. For CVOCs oxidation, surface acidity, especially the strength of Brønsted acid sites over the catalysts, was significant for TCE adsorption and degradation [62,63]. First, when the reactant passed the first part of the PtSn/CeO_2&Mn/ZSM-5 catalyst, most of the toluene was strongly adsorbed on the Pt sites and a certain amount of TCE was weakly adsorbed on the SnO_x sites. Then, toluene was oxidized into carbon dioxide and water finally. At the same time, dechlorination and chlorination occurred on the SnO_x sites throughout the entire TCE oxidation process. Second, the deep oxidation of residual TCE and Cl-containing byproducts occurred in the second part of the PtSn/CeO_2&Mn/ZSM-5. Thus, the dissociation of C—Cl and C—H bonds from the by-products proceeded normally on the second stage of the catalysts (Mn/ZSM-5). In other words, the deep oxidation of toluene and the dechlorination of TCE were relatively independent over the tandem catalysts, thus avoiding the generation of polychlorinated byproducts. However, compared to the tandem catalysts, the PtSn/CeO_2 and Mn/ZSM-5 in the physically mixed catalyst (PtSn/CeO_2+Mn/ZSM-5) contacted each other closely, which provided convenient conditions for severe electrophilic chlorination between aromatic hydrocarbons, and the Cl species desorbed from the TCE on these catalysts.

4. Conclusions

In summary, to realize the high-efficiency and safe disposal of mixed VOCs via catalytic oxidation, a promising PtSn/CeO_2&Mn/ZSM-5 tandem catalyst with favorable active sites and optimized acid sites was constructed. The former part primarily achieved the deep oxidation of toluene at low temperatures, and the doping of SnO_x changed the electronic structure around Pt and weakened the adsorption of TCE at

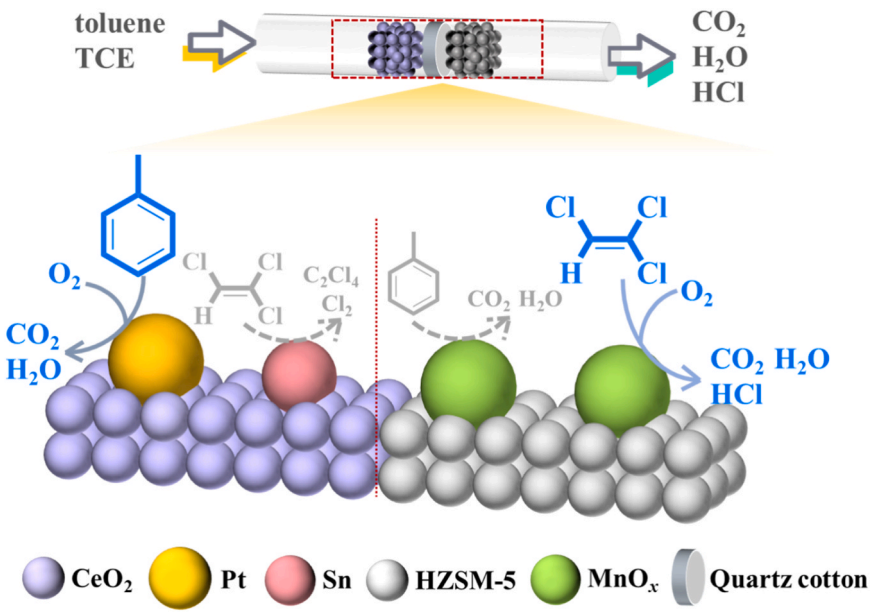

Scheme 1. An illustration of toluene and TCE oxidation mechanism over the tandem catalyst.

the Pt sites. The latter part achieved the deep oxidation of residual TCE and Cl-containing byproducts. Moreover, the PtSn/CeO_2&Mn/ZSM-5 catalyst exhibited higher catalytic activity for toluene and TCE oxidation and an excellent ability to achieve deep oxidation of the byproducts, accomplishing facile VOCs elimination and restraining the formation of polychlorinated byproducts. The tandem catalyst exhibited good stability during long-time tests in toluene and TCE mixtures, even in the presence of water; the toluene and TCE conversion remained high. This study provides a new approach for developing efficient catalysts for the mixed VOCs elimination and may inspire the utilization of the tandem catalysis technique for optimizing multicomponent VOCs degradation processes.

CRediT authorship contribution statement

Zeya Li: Investigation, Writing – review & editing. **Ruyi Gao:** Methodology, Investigation. **Zhiquan Hou:** Investigation, Data curation. **Xiaohui Yu:** Methodology, Investigation. **Hongxing Dai:** Writing – review & editing, Project administration. **Jiguang Deng:** Supervision, Formal analysis, Investigation. **Yuxi Liu:** Writing – review & editing, Supervision, Project administration.

Declaration of Competing Interest

The authors declare that they have no known competing financial interests or personal relationships that could have appeared to influence the work reported in this paper.

Data availability

No data was used for the research described in the article.

Acknowledgements

This work was financially supported by the the State's Key Project of Research and Development Plan (2022YFB3506200 and 2022YFB3504101), National Natural Science Foundation of China (21976009), National Natural Science Committee of China-Liaoning Provincial People's Government Joint Fund (U1908204), Beijing Natural Science Foundation (J210006), and R&D Program of Beijing Municipal Education Commission (KZ202210005011).

Appendix A. Supporting information

Supplementary data associated with this article can be found in the online version at doi:10.1016/j.apcatb.2023.123131.

References

[1] C. He, J. Cheng, X. Zhang, M. Douthwaite, S. Pattisson, Z. Hao, Recent advances in the catalytic oxidation of volatile organic compounds: a review based on pollutant sorts and sources, Chem. Rev. 119 (2019) 4471–4568.
[2] M. Lv, S. Song, P. Verm, M. Wen, Hollow mesoporous aluminosilicate spheres imbedded with Pd nanoparticles for high performance toluene combustion, Catal. Today 410 (2023) 135–142.
[3] S. Song, Q. Liu, J. Xiong, M. Wen, T. An, Promotional effects of Ag on catalytic combustion of cyclohexane over PdAg/Ti-SBA-15, J. Catal. 421 (2023) 77–87.
[4] F. Lin, X. Li, Z. Zhang, N. Li, B. Yan, C. He, Z. Hao, G. Chen, Comprehensive review on catalytic degradation of Cl-VOCs under the practical application conditions, Crit. Rev. Environ. Sci. Technol. 52 (2020) 311–355.
[5] G. Chen, Y. Cai, H. Zhang, D. Hong, S. Shao, C. Tu, Y. Chen, F. Wang, B. Chen, Y. Bai, X. Wang, Q. Dai, Pt and Mo co-decorated MnO_2 nanorods with superior resistance to H_2O, sintering, and HCl for catalytic oxidation of chlorobenzene, Environ. Sci. Technol. 55 (2021) 14204–14214.
[6] F. Lin, Z. Wang, Z. Zhang, L. Xiang, D. Yuan, B. Yan, Z. Wang, G. Chen, Comparative investigation on chlorobenzene oxidation by oxygen and ozone over a MnO_x/Al_2O_3 catalyst in the presence of SO_2, Environ. Sci. Technol. 55 (2021) 3341–3351.
[7] R. Peng, X. Sun, S. Li, M. Chen, M. Fu, J. Wu, Q. Dai, Shape effect of Pt/CeO_2 catalysts on the catalytic oxidation of toluene, Chem. Eng. J. 306 (2016) 1234–1246.
[8] H. Yang, J. Deng, Y. Liu, S. Xie, Z. Wu, H. Dai, Preparation and catalytic performance of Ag, Au, Pd or Pt nanoparticles supported on 3DOM CeO_2−Al_2O_3 for toluene oxidation, J. Mol. Catal. A 414 (2016) 9–18.
[9] S. Cao, X. Fei, Y. Wen, Z. Sun, H. Wang, Z. Wu, Bimodal mesoporous TiO_2 supported Pt, Pd and Ru catalysts and their catalytic performance and deactivation mechanism for catalytic combustion of dichloromethane (CH_2Cl_2), Appl. Catal. A 550 (2018) 20–27.
[10] W. Zhao, J. Cheng, L. Wang, J. Chu, J. Qu, Y. Liu, S. Li, H. Zhang, J. Wang, Z. Hao, T. Qi, Catalytic combustion of chlorobenzene on the Ln modified Co/HMS, Appl. Catal. B 127 (2012) 246–254.
[11] P. Yang, S. Zuo, Z. Shi, F. Tao, R. Zhou, Elimination of 1,2-dichloroethane over $(Ce, Cr)_xO_2/MO_y$ catalysts (M = Ti, V, Nb, Mo, W and La), Appl. Catal. B 191 (2016) 53–61.
[12] Q. Dai, L. Yin, S. Bai, W. Wang, X. Wang, X. Gong, G. Lu, Catalytic total oxidation of 1,2-dichloroethane over VO_x/CeO_2 catalysts: further insights via isotopic tracer techniques, Appl. Catal. B 182 (2016) 598–610.
[13] X. Ma, J. Wen, H. Guo, G. Ren, Facile template fabrication of Fe-Mn mixed oxides with hollow microsphere structure for efficient and stable catalytic oxidation of 1,2-dichlorobenzene, Chem. Eng. J. 382 (2020), 122940.
[14] J. Wan, P. Yang, X. Guo, R. Zhou, Investigation on the structure-activity relationship of Nb_2O_5 promoting CeO_2-CrO_2-Nb_2O_5 catalysts for 1,2-dichloroethane elimination, Mol. Catal. 470 (2019) 75–81.

[15] X. Zhang, Y. Liu, J. Deng, X. Zhao, K. Zhang, J. Yang, Z. Han, X. Jiang, H. Dai, Three-dimensionally ordered21icroporouss Cr_2O_3-CeO_2: high-performance catalysts for the oxidative removal of trichloroethylene, Catal. Today 339 (2020) 200–209.

[16] H. Zhao, F. Dong, W. Han, Z. Tang, Study of morphology-dependent and crystal-plane effects of $CeMnO_x$ catalysts for 1,2-dichlorobenzene catalytic elimination, Ind. Eng. Chem. Res. 58 (2019) 18055–18064.

[17] H. Wang, B. Peng, R. Zhang, H. Chen, Y. Wei, Synergies of Mn oxidative ability and ZSM-5 acidity for 1, 2-dichloroethane catalytic elimination, Appl. Catal. B 276 (2020), 118922.

[18] X. Weng, P. Sun, Y. Long, Q. Meng, Z. Wu, Catalytic oxidation of chlorobenzene over $Mn_xCe_{1-x}O_2$/HZSM-5 catalysts: a study with practical implications, Environ. Sci. Technol. 51 (2017) 8057–8066.

[19] P. Yang, S. Zuo, R. Zhou, Synergistic catalytic effect of $(Ce,Cr)_xO_2$ and HZSM-5 for elimination of chlorinated organic pollutants, Chem. Eng. J. 323 (2017) 160–170.

[20] X. Zhang, L. Dai, Y. Liu, J. Deng, L. Jing, Z. Wang, W. Pei, X. Yu, J. Wang, H. Dai, Effect of support nature on catalytic activity of the bimetallic RuCo nanoparticles for the oxidative removal of 1,2-dichloroethane, Appl. Catal. B 285 (2021), 119804.

[21] W. Hua, C. Zhang, Y. Guo, W. Hua, G. Chai, C. Wang, Y. Guo, L. Wang, Y. Wang, W. Zhan, An efficient $Sn_yMn_{1-y}O$ composite oxide catalyst for catalytic combustion of vinyl chloride emissions, Appl. Catal. B 255 (2019), 117748.

[22] W. Shi, Y. Quan, G. Lan, K. Ni, Y. Song, X. Jiang, C. Wang, W. Lin, Bifunctional metal−organic layers for tandem catalytic transformations using molecular oxygen and carbon dioxide, J. Am. Chem. Soc. 143 (2021) 16718–16724.

[23] H. Cho, D. Kim, J. Li, D. Su, B. Xu, Zeolite-encapsulated Pt nanoparticles for tandem catalysis, J. Am. Chem. Soc. 140 (2018) 13514–13520.

[24] T. Lohr, T. Marks, Orthogonal tandem catalysis, Nat. Chem. 7 (2015) 477–482.

[25] Y. Yamada, C. Tsung, W. Huang, Z. Huo, S. Habas, T. Soejima, C. Aliaga, G. Somorjai, P. Yang, Nanocrystal bilayer for tandem catalysis, Nat. Chem. 3 (2011) 372–376.

[26] J. Su, C. Xie, C. Chen, Y. Yu, G. Kennedy, G. Somorjai, P. Yang, Insights into the mechanism of tandem alkene hydroformylation over a nanostructured catalyst with multiple interfaces, J. Am. Chem. Soc. 138 (2016) 11568–11574.

[27] J. Kang, S. He, W. Zhou, Z. Shen, Y. Li, M. Chen, Q. Zhang, Y. Wang, Single-pass transformation of syngas into ethanol with high selectivity by triple tandem catalysis, Nat. Commun. 11 (2020) 827.

[28] S. Cao, M. Shi, H. Wang, F. Yu, X. Weng, Y. Liu, Z. Wu, Two-stage Ce/TiO_2-Cu/CeO_2 catalyst with separated catalytic functions for deep catalytic combustion of CH_2Cl_2, Chem. Eng. J. 290 (2016) 147–153.

[29] Q. Chen, Y. Yang, Z. Cao, Q. Kuang, G. Du, Y. Jiang, Z. Xie, L. Zheng, Excavated cubic platinum-tin alloy nanocrystals constructed from ultrathin nanosheets with enhanced electrocatalytic activity, Angew. Chem. Int. Ed. 55 (2016) 9021–9025.

[30] C. Shinohara, S. Kawakami, T. Moriga, H. Hayashi, S. Hodoshima, Y. Saito, S. Sugiyam, Local structure around platinum in Pt/C catalysts employed for liquid-phase dehydrogenation of decalin in the liquid-film state under reactive distillation conditions, Appl. Catal. A 266 (2004) 251–255.

[31] X. Yu, L. Dai, J. Deng, Y. Liu, L. Jing, X. Zhang, X. Jiang, Z. Hou, J. Wang, H. Dai, Catalytic performance and intermediates identification of trichloroethylene deep oxidation over Ru/3DOM SnO_2 catalysts, J. Catal. 400 (2021) 310–324.

[32] X. Weng, P. Sun, Y. Long, Q. Meng, Z. Wu, Catalytic oxidation of chlorobenzene over $Mn_xCe_{1-x}O_2$/HZSM-5 catalysts: a study with practical implications, Environ. Sci. Technol. 51 (2017) 8057–8066.

[33] D. Jin, Z. Ren, Z. Ma, F. Liu, H. Yang, Low temperature chlorobenzene catalytic oxidation over MnO_x/CNTs with the assistance of ozone, RSC Adv. 5 (2015) 15103–15109.

[34] K. Cao, X. Dai, Z. Wu, X. Weng, Unveiling the importance of reactant mass transfer in environmental catalysis: taking catalytic chlorobenzene oxidation as an example, Chin. Chem. Lett. 32 (2021) 1206–1209.

[35] C. Baranowski, A. Bahmanpour, F. Héroguel, J. Luterbacher, O. Kröcher, Prominent role of mesopore surface area and external acid sites for the synthesis of polyoxymethylene dimethyl ethers (OME) on a hierarchical H-ZSM-5 zeolite, Catal. Sci. Technol. 9 (2019) 366–376.

[36] H. Wang, B. Peng, R. Zhang, H. Chen, Y. Wei, Synergies of Mn oxidative ability and ZSM-5 acidity for 1, 2-dichloroethane catalytic elimination, Appl. Catal. B 276 (2020), 118922.

[37] C. Chen, X. Wang, J. Zhang, S. Pan, C. Bian, L. Wang, F. Chen, X. Meng, X. Zheng, X. Gao, F. Xia, Superior performance in catalytic combustion of toluene over KZSM-5 zeolite supported platinum catalyst, Catal. Lett. 144 (2014) 1851–1859.

[38] P. Bera, K. Priolkar, A. Gayen, P. Sarode, M. Hegde, S. Emura, R. Kumashiro, V. Jayaram, G. Subbanna, Ionic dispersion of Pt over CeO_2 by the combustion method: structural investigation by XRD, TEM, XPS, and EXAFS, Chem. Mater. 15 (2003) 2049–2060.

[39] Q. Zhang, S. Mo, J. Li, Y. Sun, M. Zhang, P. Chen, M. Fu, J. Wu, L. Chen, D. Ye, In situ DRIFT spectroscopy insights into the reaction mechanism of CO and toluene co-oxidation over Pt-based catalysts, Catal. Sci. Technol. 9 (2019) 4538–4551.

[40] R. Peng, X. Sun, S. Li, L. Chen, M. Fu, J. Wu, D. Ye, Shape effect of Pt/CeO_2 catalysts on the catalytic oxidation of toluene, Chem. Eng. J. 306 (2016) 1234–1246.

[41] Y. Feng, L. Wei, Z. Wang, Y. Liu, H. Dai, C. Wang, H. Hsi, E. Duan, Y. Peng, J. Deng, Boosting catalytic stability for VOCs removal by constructing PtCu alloy structure with superior oxygen activation behavior, J. Hazard. Mater. 439 (2022), 129612.

[42] T. Gan, X. Chu, H. Qi, W. Zhang, Y. Zou, W. Yan, G. Liu, Pt/Al_2O_3 with ultralow Pt-loading catalyze toluene oxidation: promotional synergistic effect of Pt nanoparticles and Al_2O_3 support, Appl. Catal. B 257 (2019), 117943.

[43] S. Li, Y. Lin, D. Wang, C. Zhang, Z. Wang, X. Li, Polyhedral cobalt oxide supported Pt nanoparticles with enhanced performance for toluene catalytic oxidation, Chemosphere 263 (2021), 127870.

[44] S. Cao, X. Fei, Y. Wen, Z. Sun, H. Wang, Z. Wu, Bimodal mesoporous TiO_2 supported Pt, Pd and Ru catalysts and their catalytic performance and deactivation mechanism for catalytic combustion of Dichloromethane (CH_2Cl_2), Appl. Catal. A 550 (2018) 20–27.

[45] C. Chen, F. Chen, L. Zhang, S. Pan, C. Bian, X. Zheng, X. Meng, F. Xiao, Importance of platinum particle size for complete oxidation of toluene over Pt/ZSM-5 catalysts, Chem. Commun. 51 (2015) 5936–5938.

[46] M. i, D. Fino, N. Russo, Mesoporous manganese oxides prepared by solution combustion synthesis as catalysts for the total oxidation of VOCs, Appl. Catal. B 163 (2015) 277–287.

[47] Z. Qu, Y. Bu, Y. Qin, Y. Wang, Q. Fu, The improved reactivity of manganese catalysts by Ag in catalytic oxidation of toluene, Appl. Catal. B 132–133 (2013) 353–362.

[48] Z. Li, J. Liu, B. Gao, L. Bo, Cu-Mn-CeO_x loaded ceramic catalyst for non-thermal sterilization and microwave thermal catalysis of VOCs degradation, Chem. Eng. J. 442 (2022), 136288.

[49] D. Xia, H. Liu, B. Xu, Y. Wang, Y. Liao, Y. Huang, L. Ye, C. He, P. Wong, R. Qiu, Single Ag atom engineered 3D-MnO_2 porous hollow microspheres for rapid photothermocatalytic inactivation of *E. coli* under solar light, Appl. Catal. B 245 (2019) 177–189.

[50] P. Sun, W. Wang, X. Weng, X. Dai, Z. Wu, Alkali potassium induced HCl/CO_2 selectivity enhancement and chlorination reaction inhibition for catalytic oxidation of chloroaromatics, Environ. Sci. Technol. 52 (2018) 6438–6447.

[51] Y. Shua, M. He, J. Jia, H. Huang, S. Liu, D. Leung, Synergetic degradation of VOCs by vacuum ultraviolet photolysis and catalytic ozonation over Mn-*x*Ce/ZSM-5, J. Hazard. Mater. 364 (2019) 770–779.

[52] Y. Fang, Q. Zhang, H. Zhang, X. Li, W. Chen, J. Xu, H. Shen, J. Yang, C. Pan, Y. Zhu, J. Wang, Z. Luo, L. Wang, X. Bai, F. Song, L. Zhang, Y. Guo, Dual activation of molecular oxygen and surface lattice oxygen in single atom Cu_1/TiO_2 catalyst for CO oxidation, Angew. Chem. Int. Ed. 61 (2022), e202212273.

[53] R. Behm, C. Brundle, On the formation and bonding of a surface carbonate on Ni (100), Surf. Sci. 255 (1991) 327–343.

[54] D. Zhao, G. Sheng, C. Chen, X. Wang, Enhanced photocatalytic degradation of methylene blue under visible irradiation on graphene@TiO_2 dyade structure, Appl. Catal. B 111–112 (2012) 303–308.

[55] T. Frantz, W. Ruiz, C. Rosa, V. Mortola, Synthesis of ZSM-5 with high sodium content for CO_2 adsorption, Microporous Mesoporous Mater. 222 (2016) 209e217.

[56] S. Bai, B. Shi, W. Deng, Q. Dai, X. Wang, Catalytic oxidation of 1,2-dichloroethane over Al_2O_3–CeO_2 catalysts: combined effects of acid and redox properties, RSC Adv. 5 (2015) 48916–48927.

[57] X. Liu, L. Chen, T. Zhu, R. Ning, Catalytic oxidation of chlorobenzene over noble metals (Pd, Pt, Ru, Rh) and the distributions of polychlorinated by-products, J. Hazard. Mater. 363 (2019) 90–98.

[58] M. Wen, S. Song, W. Zhao, Q. Liu, J. Chen, G. Li, T. An, Atomically dispersed Pd sites on Ti-SBA-15 for efficient catalytic combustion of typical gaseous VOCs, Environ. Sci. Nano 8 (2021) 3735–3745.

[59] R. López-Fonseca, A. Aranzabal, J. Gutiérrez-Ortiz, J. Álvarez-Uriarte, J. González-Velasco, Comparative study of the oxidative decomposition of trichloroethylene over H-type zeolites under dry and humid conditions, Appl. Catal. B 30 (2001) 303–313.

[60] M. Tian, Z. Jiang, C. Chen, M. Kosari, X. Li, Y. Jian, Y. Huang, J. Zhang, L. Li, J. Shi, Y. Zhao, C. He, Engineering Ru/$MnCo_3O_x$ for 1,2-dichloroethane benign destruction by strengthening C−Cl cleavage and chlorinedesorption: decisive role of H_2O and reaction mechanism, ACS Catal. 12 (2022) 8776–8792.

[61] C. Chen, F. Chen, L. Zhang, S. Pan, C. Bian, X. Zheng, X. Meng, F. Xiao, Importance of platinum particle size for complete oxidation of toluene over Pt/ZSM-5 catalysts, Chem. Commun. 51 (2015) 5936–5938.

[62] Z. Zhang, H. Xia, Q. Dai, X. Wang, Dichloromethane oxidation over Fe_xZr_{1-x} oxide catalysts, Appl. Catal. A 557 (2018) 108–118.

[63] K. Goła¸bek, A. Palomares, J. Martınez-Triguero, K. Tarach, K. Kruczała, V. Girman, K. Gora-Marek, Ce-modified zeolite BEA catalysts for the trichloroethylene oxidation. The role of the different and necessary active sites, Appl. Catal. B 259 (2019) 118022–118033.